

HST PHOTOMETRY AND KECK SPECTROSCOPY OF THE RICH CLUSTER MS 1054-03: MORPHOLOGIES,  
BUTCHER-OEMLER EFFECT AND THE COLOR-MAGNITUDE RELATION AT  $Z = 0.83$ <sup>1,2</sup>PIETER G. VAN DOKKUM<sup>3</sup> AND MARIJN FRANX

Leiden Observatory, P.O. Box 9513, NL-2300 RA, Leiden, The Netherlands

DANIEL FABRICANT

Harvard-Smithsonian Center for Astrophysics, 60 Garden Street, Cambridge, MA 02318

GARTH D. ILLINGWORTH

University of California Observatories/Lick Observatory, University of California, Santa Cruz, CA 95064

AND

DANIEL D. KELSON

D. T. M., Carnegie Institution of Washington, 5241 Broad Branch Road, NW, Washington DC, 20015

*Accepted for publication in the Astrophysical Journal*

## ABSTRACT

We present a study of 81 *I*-band selected, spectroscopically-confirmed members of the X-ray cluster MS 1054-03 at  $z = 0.83$ . Redshifts and spectral types were determined from Keck spectroscopy. Morphologies and accurate colors were determined from a large mosaic of HST WFPC2 images in  $R_{F606W}$  and  $I_{F814W}$ , corresponding to *U* and *B* in the restframe. Early-type galaxies constitute only 44 % of this galaxy population. This fraction is much lower than in comparable rich clusters at low redshift. Thirty-nine percent are spiral galaxies, and 17 % are mergers. The early-type galaxies follow a tight and well-defined color-magnitude relation, with the exception of a few outliers. The observed scatter is  $0.029 \pm 0.005$  magnitudes in restframe  $U - B$ . Most of the mergers lie close to the CM relation defined by the early-type galaxies. They are bluer by only  $0.07 \pm 0.02$  magnitudes, and the scatter in their colors is  $0.07 \pm 0.04$  magnitudes. Spiral galaxies in MS 1054-03 exhibit a large range in their colors. The bluest spiral galaxies are  $\sim 0.7$  magnitudes bluer than the early-type galaxies, but the majority is within  $\pm 0.2$  magnitudes of the early-type galaxy sequence. The red colors of the mergers and the majority of the spiral galaxies are reflected in the fairly low Butcher-Oemler blue fraction of MS 1054-03:  $f_B = 0.22 \pm 0.05$ , similar to intermediate redshift clusters and much lower than previously reported values for clusters at  $z \sim 0.8$ . The slope and scatter of the CM relation of early-type galaxies are roughly constant with redshift, confirming previous studies that were based on ground-based color measurements and very limited membership information. However, the scatter in the combined sample of early-type galaxies and mergers (i.e., the sample of *future* early-type galaxies) is twice as high as the scatter of the early-type galaxies alone. This is a direct demonstration of the “progenitor bias”: high redshift early-type galaxies seem to form a homogeneous, old population because the progenitors of the youngest present-day early-type galaxies are not included in the sample.

*Subject headings:* galaxies: evolution, galaxies: elliptical and lenticular, cD, galaxies: structure of, galaxies: clusters: individual (MS 1054-03)

## 1. INTRODUCTION

The star formation history of early-type galaxies provides an important constraint on models for galaxy formation and a test for stellar population synthesis models. Because present-day early-type galaxies consist mostly of old stars, the evolution of their stellar populations may provide clues to conditions in the early Universe. Early-type galaxies (elliptical galaxies and S0 galaxies) are very efficiently studied in clusters. They form the dominant population in nearby rich clusters (Oemler 1974; Dressler 1980), and most of our knowledge of the formation and evolution of early-type galaxies has come from studies of clusters at  $0 < z < 0.5$ .

Strong constraints on the star formation histories of early-type galaxies have been derived from the redshift evolution of the Fundamental Plane relation (van Dokkum & Franx 1996, Kelson et al. 1997, Pahre 1998, Bender et al. 1998, van Dokkum

et al. 1998b, Jørgensen et al. 1999, Kelson et al. 2000) and the color-magnitude relation (e.g., Ellis et al. 1997, Stanford, Eisenhardt, & Dickinson 1998, van Dokkum et al. 1998a, Kodama et al. 1998). The strongest constraints on the *mean* star formation epoch are provided by the evolution of the Fundamental Plane, mainly because the mean luminosity evolution is large compared to the mean color evolution. van Dokkum et al. (1998b) find a slow luminosity evolution of early-type galaxies to  $z = 0.83$ , and conclude that their stars were formed at  $z > 2.8$  for a Salpeter (1955) IMF,  $\Omega_m = 0.3$  and  $\Omega_\Lambda = 0$ , or  $z > 1.7$  for  $\Omega_m = 0.3$  and  $\Omega_\Lambda = 0.7$ .

Whereas the Fundamental Plane can be used to measure the mean luminosity evolution of early-type galaxies with high accuracy, it is difficult to obtain a sufficiently large sample to study the evolution of its slope and scatter (but not impossible, see Kelson et al. 2000). Furthermore, the Fundamental

<sup>1</sup>Based on observations with the NASA/ESA *Hubble Space Telescope*, obtained at the Space Telescope Science Institute, which is operated by AURA, Inc., under NASA contract NAS 5-26555.

<sup>2</sup>Based on observations obtained at the W. M. Keck Observatory, which is operated jointly by the California Institute of Technology and the University of California.

<sup>3</sup>Present address: California Institute of Technology, MS 105-24, Pasadena, CA 91125

Plane can only be applied to early-type galaxies, and concentrating on the early-type galaxy population alone may lead to an incomplete picture of their evolution. There is growing evidence that a significant fraction of present-day early-type galaxies was assembled relatively recently (Dressler et al. 1997; van Dokkum et al. 1999). They may have formed from gas stripping of spiral galaxies (e.g., Gunn & Gott 1972, Tytler & Vidal 1978, Solanes & Salvador-Sole 1992, Couch et al. 1998, Abadi, Moore, & Bower 1999), through tidal interactions (e.g., Fried 1988, Lavery, Pierce, & McClure 1992, Oemler, Dressler, & Butcher 1997, Moore, Lake, & Katz 1998, Couch et al. 1998), or in mergers (e.g., Lavery et al. 1992, van Dokkum et al. 1999). Early-type galaxies in high redshift clusters may therefore form a special subset of the progenitors of early-type galaxies in nearby clusters. Failure to consider the other progenitors may result in biased age estimates (see, e.g., Franx & van Dokkum 1996).

The evolution of the color-magnitude (CM) relation can provide important constraints additional to those provided by the Fundamental Plane. The CM relation is useful for studying all morphological types and large photometric samples can be obtained straightforwardly. The combination of the mean color evolution of galaxies and their luminosity evolution can constrain the IMF (e.g., Kelson et al. 2000). The evolution of the slope of the CM relation is sensitive to age differences between high mass galaxies and low mass galaxies (see, e.g., Kodama et al. 1998). The scatter in the CM relation is particularly important. It can be measured to high accuracy with HST and it constrains the age spread of galaxies of a given luminosity (Bower, Lucey, & Ellis 1992; Ellis et al. 1997; van Dokkum et al. 1998a; Stanford et al. 1998). The scatter is proportional to  $\Delta \ln(\tau) = \Delta \tau / \langle \tau \rangle$ , where  $\tau$  is the luminosity-weighted age (see van Dokkum et al. 1998a).

The evolution of the color-magnitude relation has been studied extensively (e.g., Aragon-Salamanca et al. 1993, Stanford, Eisenhardt, & Dickinson 1995, Ellis et al. 1997, Stanford et al. 1998, Kodama et al. 1998). These studies are in remarkable agreement: the slope and scatter seem to be roughly constant with redshift, and the mean color evolution is consistent with passive evolution of an old stellar population that was formed at high redshift. However, these studies suffer from limited membership information and areal coverage (usually one HST+WFPC2 pointing). Because the field contamination among late-type galaxies becomes very large at  $z \sim 1$  usually only early-type galaxies are considered, and even these morphologically selected samples suffer from significant contamination. For example, Stanford et al. (1998) estimate that the field contamination among the early-type galaxies in their  $z > 0.6$  clusters is 20–40%, depending on the richness of the cluster. An additional complication is that the true contamination is expected to vary considerably on the small angular scales of the fields used for these studies.

We are undertaking a program to obtain large field HST+WFPC2 mosaics of clusters at  $0.3 < z < 1$ , combined with extensive spectroscopy from the ground. This program is complimentary to other HST studies of distant clusters, in the sense that we observe only a few clusters, but over a large field and with redshifts for  $\gtrsim 200$  (field and cluster) galaxies for each cluster field. The CM relation in the cluster CL 1358+62 at  $z = 0.33$  was presented by van Dokkum et al. (1998a). We used a sample of 194 confirmed members observed with HST. It was found that S0 galaxies in the outskirts of the cluster show a

much larger scatter in their colors and are bluer on average than those in the central regions, providing evidence for recent infall of galaxies from the field. Here, we present extensive Keck spectroscopy and a large HST WFPC2 mosaic in two filters of the cluster MS 1054–03 at  $z = 0.83$ . Redshifts, morphologies and accurate colors are presented for a sample of 81 confirmed cluster members. One of the most striking results of our survey is the large number of merging systems in MS 1054–03 (van Dokkum et al. 1999). In the present study we focus on the CM relation of confirmed members. The aims are to test whether the early-types are a homogeneous population at  $z \approx 1$ , and to compare their CM relation to those of other morphological types.

## 2. DATA

### 2.1. Spectroscopy

The spectroscopic survey of the MS 1054–03 field used the LRIS spectrograph (Oke et al. 1995) on the 10 m W. M. Keck II Telescope. The primary purpose of the survey was to obtain a sample of  $I$ -band selected, spectroscopically confirmed cluster galaxies.

#### 2.1.1. Sample Selection and Observations

Targets for the spectroscopy were selected from a photometric catalog of objects in the MS 1054–03 field. The catalog was created from a 900 s Keck  $I$ -band image of the cluster, centered on the Brightest Cluster Galaxy (BCG), and spanning  $5' \times 7'$ . The seeing in the image is  $1.^{\prime\prime}0$  FWHM. Objects were detected with FOCAS (Valdes et al. 1995).  $I$  band magnitudes were measured through  $3''$  diameter apertures. The 412 objects in the catalog with  $20.0 < I < 22.7$  were selected as potential targets for the spectroscopy. The  $I$  magnitude of the BCG equals 20.2. Six slitmasks were designed, with  $\sim 40$  slitlets each. Objects in the magnitude range  $20.0 < I < 22.2$  were given the highest priority. Objects located outside the boundaries of our HST mosaic were given low priority irrespective of their magnitude. The positions and position angles of the masks maximize the total number of slitlets within the area covered by our HST imaging.

The MS 1054–03 field was observed 1998 February 28 and March 1. All six slitmasks were exposed, using the  $400 \text{ mm}^{-1}$  grating blazed at  $8500 \text{ \AA}$ , and  $1.^{\prime\prime}2$  wide slits. Five masks were exposed for  $2 \times 1200$  s, and one mask for 1200 s. The seeing was  $\approx 0.^{\prime\prime}8$  during the observations. The instrumental resolution, as measured from sky lines, is  $\approx 7 \text{ \AA}$  FWHM at  $7500 \text{ \AA}$ . The wavelength coverage depends on the position of each slitlet in the multislit mask, but is typically  $5700 - 9500 \text{ \AA}$ . The  $[\text{O II}]$   $3727 \text{ \AA}$  doublet and the  $4000 \text{ \AA}$  break redshifted to  $z = 0.83$  are covered in all slitlets. The data reduction is described in Appendix A.1.

#### 2.1.2. Redshifts and Completeness

A total of 256 1D spectra were extracted from the 2D data. This number includes serendipitous detections. We calculated the sampling rate by dividing the number of objects in the spectroscopic sample by the number of objects in the photometric catalog. Figure 1(a) shows the sampling rate as a function of magnitude, calculated in  $\pm 0.25$  magnitude bins around each galaxy. Approximately 90% of all  $I \approx 21$  objects within the boundaries of our HST mosaic were observed. The sampling rate drops precipitously at  $I \gtrsim 22$ , consistent with our selection process.

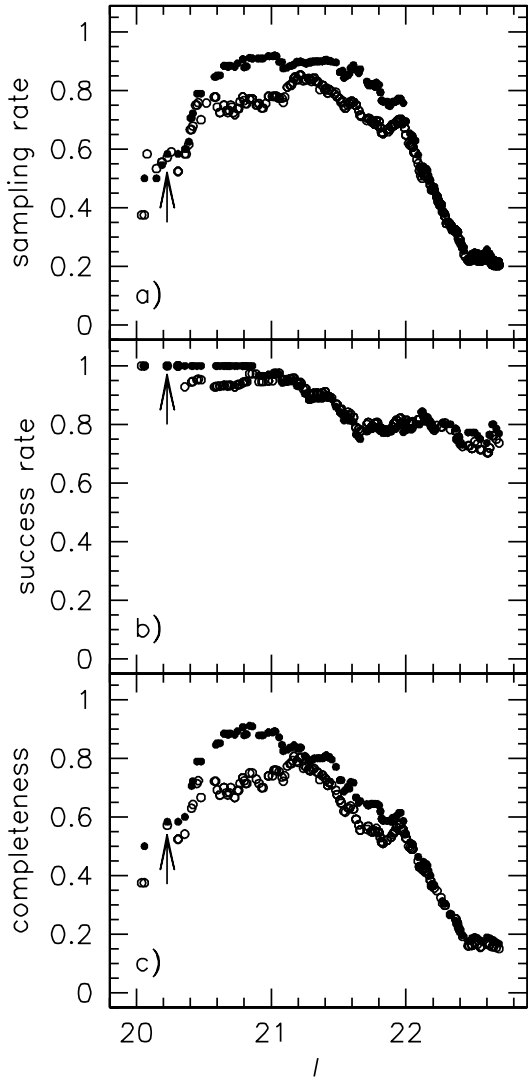


Fig. 1.— (a) The sampling rate as a function of magnitude, calculated by dividing the number of galaxies in our spectroscopic sample by the number of galaxies in the photometric catalog, in  $\pm 0.25$  mag bins centered on each galaxy. Open symbols are for the full sample, solid symbols for objects covered by our HST imaging. The arrow indicates the BCG. (b) The success rate of measuring the redshift of observed objects. The success rate is still  $\approx 80\%$  at  $I = 22.7$ . (c) The completeness, calculated by dividing the number of galaxies with measured redshift by the number of galaxies in the photometric catalog. At a given magnitude, the completeness is the product of the sampling rate and the success rate. The incompleteness at the faint end of the sample is primarily caused by sparse sampling, and not by the inability to measure redshifts of observed galaxies.

Redshifts were measured from emission lines using SPLIT in IRAF, or determined from absorption lines using the cross-correlation routine XCDAO. For the cross-correlations two template spectra were used: the spectrum of the nearby early-type galaxy NGC 7331, and the spectrum of the E+A galaxy 209 in CL 1358+62 (Fisher et al. 1998). The galaxies and the templates were cross-correlated in the 3750 – 4500 Å restframe wavelength range. Redshifts were determined for 200 objects. Ten turned out to be stars, and four were observed twice. Therefore, the number of galaxies with redshifts is 186. The success rate of measuring the redshift of observed objects is shown in

Fig. 1(b). The success rate is still as high as  $\approx 80\%$  at  $I = 22.7$ .

We investigate the completeness of the spectroscopic sample by comparing the number of galaxies with measured redshifts to the number of galaxies in the photometric catalog. Figure 1(c) shows the completeness (or the “magnitude selection function”, cf. Yee et al. 1996) as a function of  $I$  magnitude. The sample is 65% complete for  $20.0 < I < 22.2$ , and 16% complete for  $22.2 \leq I < 22.7$ . Within the boundaries of the HST mosaic the completeness is 73% for  $20.0 < I < 22.2$ , and 17% for  $22.2 \leq I < 22.7$ . As is often the case in this type of survey (e.g., Lilly 1993, Fisher et al. 1998) the incompleteness at the faint end of the sample is primarily caused by sparse sampling, and not by the inability to measure redshifts of observed galaxies.

An important question is whether there is a color bias in the sample of galaxies with redshifts. In Fig. 2(a) the distribution of  $R - I$  colors is shown for the full photometric sample, in the magnitude range  $22.2 \leq I < 22.7$ . The  $R$  magnitudes were determined from an image kindly provided by G. Luppino (Luppino & Kaiser 1997); the  $R - I$  colors were normalized to the colors of the BCG. Figure 2(b) shows the color distribution for the sample of galaxies with redshifts (solid line). As a result of the sparse sampling at faint magnitudes there is a small bias against blue galaxies in the spectroscopic sample.

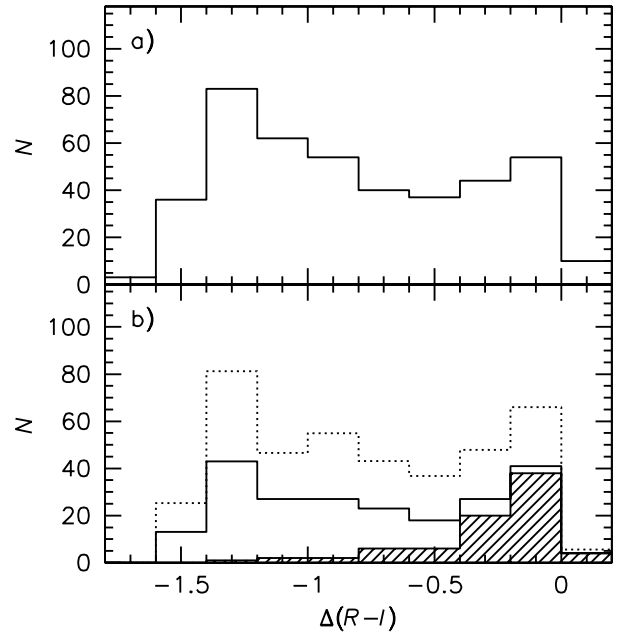


Fig. 2.— (a) Color distribution of all galaxies in the photometric catalog. (b) Color distribution of galaxies with a measured redshift (solid histogram). The broken histogram is the same distribution, corrected for incompleteness (see text). The hatched histogram shows the color distribution of confirmed cluster members.

We test whether there is an additional source of color bias in the spectroscopic sample by assigning each galaxy a weight equal to the inverse of the magnitude selection function shown in Fig. 1(c). The resulting distribution is shown by the broken line in Fig. 2(b), and is very similar to the color distribution of the full photometric sample shown in Fig. 2(a). We conclude that there is no bias against blue galaxies in the spectroscopic sample after correcting for the sparse sampling at faint magnitudes. We note that the effect of this completeness correction

is small for the cluster galaxies. The hatched histogram in Fig. 2(b) shows the color distribution of confirmed cluster galaxies. Among blue galaxies with measured redshifts the fraction of cluster members is very low. We will return to this issue in Sect. 5.3.

### 2.1.3. Redshift Distribution and Velocity Dispersion

Figure 3 shows the redshift distribution of our sample of 186 galaxies. The peak at  $z = 0.83$  is conspicuous, and MS 1054-03 is well separated from the field in redshift space. In the redshift range  $0.78 < z < 0.87$  all galaxies have redshifts in the interval  $0.8132 < z < 0.847$ , i.e., within  $\pm 2.7 \sigma_{\text{cl}}$  (Tran et al. 1999). The separation of cluster galaxies and field galaxies is therefore straightforward.

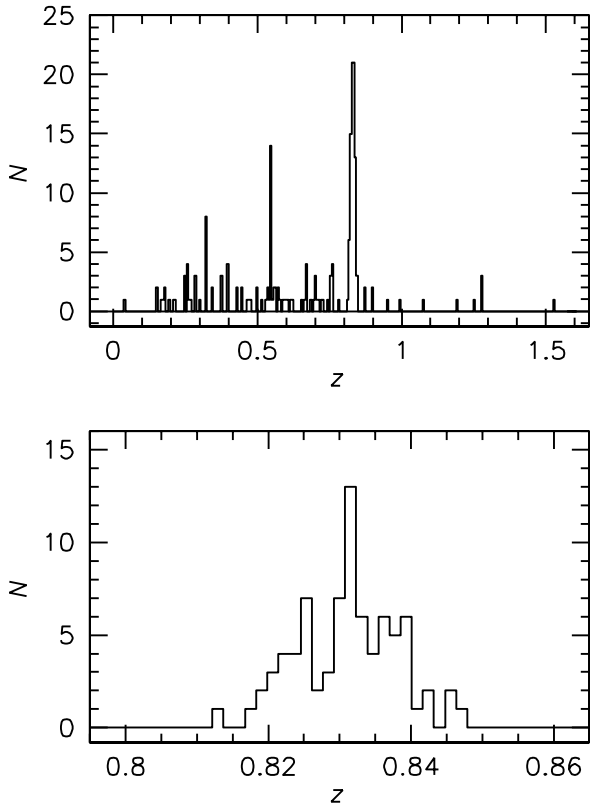


Fig. 3.— Redshift distribution of galaxies in our spectroscopic sample. The peak at  $z = 0.83$  is conspicuous, and well separated from the field. We find at least two peaks at lower redshifts.

There are 78 cluster members in our spectroscopic sample. Two additional cluster members were observed serendipitously, in slits pointed at other objects. These galaxies with  $I \sim 24$  will not be considered in subsequent analysis. Redshifts of cluster members are listed in Table 1 in Appendix A. Uncertainties in radial velocity are typically  $\sim 30 \text{ km s}^{-1}$  in the restframe ( $\Delta z \sim 0.0002$ ). We can refine the Donahue et al. (1998) and Tran et al. (1999) determinations of the mean redshift and velocity dispersion of MS 1054-03. Using the biweight estimators for location and scale (Beers, Flynn, & Gebhardt 1990) we find  $\langle z \rangle = 0.8315 \pm 0.0007$  and  $\sigma = 1150 \pm 97 \text{ km s}^{-1}$  for our sample of 78 members. The uncertainty in  $\sigma$  was determined from bootstrap resampling.

### 2.1.4. Spectral Types

We determined spectral types of the cluster galaxies from the strengths of the [O II] 3727 Å emission line and the H $\delta$  4102 Å Balmer line. The procedure is described in Appendix A.2. In our restframe  $B$  selected sample of 78 cluster galaxies, there are 52 absorption line galaxies (67 %), 15 emission line galaxies (19 %), and 11 E+A galaxies (14 %). These fractions are somewhat uncertain due to the large number of galaxies which are less than  $1\sigma$  removed from other spectral types. The number fractions of the various spectral types are not significantly different from those in intermediate redshift clusters (e.g., Couch & Sharples 1987, Balogh et al. 1998, Fisher et al. 1998, Poggianti et al. 1999). The fraction of emission line galaxies in MS 1054-03 is significantly lower than that of the optically selected massive cluster CL 1604+4304 at  $z = 0.89$ , as determined by Postman, Lubin, & Oke (1998). These authors find that 11 out of 22 cluster galaxies have  $\text{EW} [\text{O II}] > 15 \text{ Å}$ . In contrast, only 7 out of 78 galaxies in MS 1054-03 have  $\text{EW} [\text{O II}] > 15 \text{ Å}$ . We note, however, that the Postman et al. (1998) sample extends to fainter magnitudes than our sample. Furthermore, our sample was selected in restframe  $B$  and the Postman et al. (1998) sample in restframe  $U$ . Finally, CL 1604+4304 is an optically selected cluster whereas MS 1054-03 was selected because of its high X-ray luminosity.

The emission line galaxies in MS 1054-03 are less concentrated toward the center of the cluster than the other galaxies. The fraction of emission line galaxies is 6 % within a radius of  $0.5 h_{50}^{-1} \text{ Mpc}$ , and 31 % outside  $R = 0.5 h_{50}^{-1} \text{ Mpc}$ . These numbers are similar to those found for low and intermediate redshift clusters (e.g., de Theije & Katgert 1999, Balogh et al. 1998).

We combine the new redshifts with samples of Donahue et al. (1998) and Tran et al. (1999), giving a total number of 89 spectroscopically confirmed cluster members. For subsequent analysis, we use the 81 confirmed members that are covered by our HST imaging.

## 2.2. HST WFPC2 Imaging

We have obtained a large HST WFPC2 mosaic of MS 1054-03, consisting of six slightly overlapping pointings. The area of the mosaic is  $25 \text{ arcmin}^2$ , or  $8 h_{50}^{-2} \text{ Mpc}^2$ . MS 1054-03 was observed with the F606W and F814W filters on 1998 May 30. Exposure times were 6500 s in each passband and at each position. The images were interlaced to improved the sampling by a factor  $\sqrt{2}$ . Interlacing leaves the pixel values intact, and there is no loss of information. The reduction and interlacing procedures are described in Appendix B. A color image of the mosaic is shown in Fig. 4. The red cluster galaxies stand out, and the irregular structure of the cluster is obvious.

Restframe  $B_z$  magnitudes and accurate  $(U - B)_z$  colors for the eighty-one cluster members were determined from the HST mosaic, as described in Appendix B. Magnitudes and colors of these galaxies are listed in Table 2 in Appendix B.

## 3. MORPHOLOGIES

### 3.1. Visual Classifications

The F814W WFPC2 images of the 81 confirmed members in the HST mosaic were visually classified by three of us (PGvD, MF, and DF). Details of the classification procedure can be found in Fabricant, Franx, & van Dokkum (2000). In summary, the images were compared to images of nearby galaxies from

Figure available from  
<http://astro.caltech.edu/~pgd/cm1054/fig4.eps.gz>

Fig. 4.— Hubble Space Telescope WFPC2 mosaic of the cluster MS 1054–03 at  $z = 0.83$ . This color image was created from the F606W and F814W exposures, and spans roughly  $4' \times 6'$  ( $2 \times 3 h_{50}^{-1}$  Mpc). The red cluster galaxies are conspicuous. Note their irregular and elongated distribution.

the survey by Jansen et al. (2000). The classification system is identical to that of Fabricant et al. (2000), and similar to the system of Smail et al. (1997). In order to extract as much information as possible from our data the galaxies were displayed at both the original  $0.^{\circ}1$  WFC resolution, and the  $0.^{\circ}071$  resolution of the interlaced images. The three sets of classifications were compared to assess their internal errors. In general, classifications agreed within the broad categories of early-type galaxy, spiral galaxy, or merger. If galaxy types are binned in the two categories early-types (E, E/S0, S0) and other types the three classifiers agreed on 76 % of all galaxies. To combine the classifications we used the same combination rules as Fabricant et al. (2000). The resulting classifications are listed in Table 2 in Appendix B.

### 3.2. The Early-Type Galaxy Fraction

The relative fractions of elliptical galaxies, S0 galaxies, spiral galaxies, and mergers are 22 %, 22 %, 39 %, and 17 % respectively, where E/S0 galaxies and S0/a galaxies are evenly split between their neighboring types. The ratio of elliptical galaxies to S0 galaxies is  $\sim 1$ . This quantity is somewhat uncertain as it is very difficult to distinguish elliptical galaxies from S0 galaxies (see Sect. 3.3). The fraction of early-type galaxies (E+E/S0+S0) is usually better determined (e.g., Fabricant et al. 2000). Only 34 out of 77 classified galaxies (44 %) are early-type galaxies. This number includes 50 % of galaxies classified as S0/a.

This low early-type fraction is surprising, because the projected galaxy density of MS 1054–03 is very high. We calculated the projected galaxy density following the prescription of Dressler (1980). The average galaxy density  $\log \rho_{\text{proj}} \approx 1.5 h_{50}^{-2} \text{ Mpc}^{-2}$  within a circular aperture of radius  $120''$  centered on the Brightest Cluster Galaxy (BCG). This aperture contains 87 % of our 81 confirmed members. The logarithm of the average projected density rises to  $\approx 1.8 h_{50}^{-1} \text{ Mpc}^{-2}$  in the central  $60''$  ( $570 h_{50}^{-1} \text{ kpc}$ ). At low redshift, early-type galaxies constitute  $\sim 80$  % of the galaxy population in regions with such high galaxy densities (Dressler 1980), much higher than the value of 44 % we find for MS 1054–03 at  $z = 0.83$ .

In Fig. 5 we test whether the fraction of early-type galaxies in MS 1054–03 is a function of  $R$ , the projected distance from the BCG. The histogram shows the average early-type fraction in  $0.5 h_{50}^{-1} \text{ Mpc}$  wide bins. The early-type fraction is constant at  $R \lesssim 1 h_{50}^{-1} \text{ Mpc}$ , and may decline outside this radius. There is no rise of the early-type fraction in the central regions of the cluster, contrary to what is seen in low redshift clusters (Dressler 1980).

MS 1054–03 has an irregular and elongated appearance (see Hoekstra, Franx, & Kuijken 2000 and Fig. 4). We test whether the low early-type fraction in the central regions of MS 1054–03 is related to substructure, by calculating the early-type fraction within apertures centered on the three most luminous galaxies in the cluster. Their positions coincide with the three strongest peaks in the luminosity density distribution. The early-type fractions in the immediate vicinity of these three galaxies are in fact somewhat lower than the average fraction in the central region of the cluster: they are 33 %, 38 % and 38 % within circles with radii  $R = 0.25 h_{50}^{-1} \text{ Mpc}$  centered on galaxies 1484, 1325 and 1405 respectively. We conclude that even in the highest density regions of the cluster the fraction of early-type galaxies does not exceed 50 %.

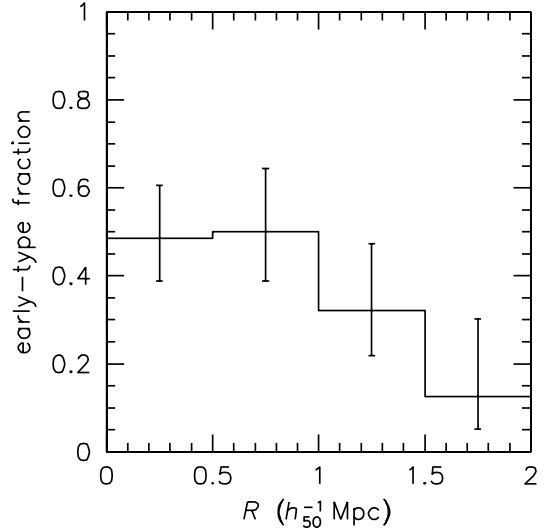


Fig. 5.— Early-type fraction plotted against  $R$ , the projected distance from the BCG. The histogram shows the average early-type fraction in  $0.5 h_{50}^{-1} \text{ Mpc}$  wide bins. The early-type fraction is low, even in the central regions of the cluster.

### 3.3. The Early-Type Fraction in Rich Clusters from $z = 0$ to $z = 1$

We can compare the fraction of early-type galaxies in MS 1054–03 to the fractions in other clusters. The evolution of the early-type fraction is shown in Fig. 6. The large symbols are CL1358+62 at  $z = 0.33$  and MS 1054–03 at  $z = 0.83$ . For CL1358+62 we used the sample of confirmed members presented in Fisher et al. (1998) and van Dokkum et al. (1998a), with morphological classifications from Fabricant et al. (2000). For consistency with Dressler et al. (1997) we computed the early-type fraction in these clusters within the physical radius that corresponds to one WFPC2 pointing at  $z = 0.45$  ( $R = 600 h_{50}^{-1} \text{ kpc}$ ). The star symbol at  $z = 0.04$  represents the concentrated clusters from Dressler (1980), taking the revised morphological fractions from Dressler et al. (1997). Triangles are from Andreon, Davoust, & Heim (1997) and small circles from Dressler et al. (1997). The connected symbols at  $z = 0.41$  are for CL0939+47, which was classified both by Andreon et al. and Dressler et al. The cross is CL1358+62 at  $z = 0.33$ , as classified by A. Dressler (see Fabricant et al. 2000). The square at  $z = 0.90$  is derived from twelve confirmed members of the cluster CL1604+43 (Lubin et al. 1998). Filled symbols indicate clusters with  $L_X > 10^{44.5} h_{50}^{-2} \text{ ergs s}^{-1}$ . X-ray luminosities are taken from Fabricant, McClintock, & Bautz (1991), Smail et al. (1997), Donahue et al. (1998), and Postman et al. (1998).

There is a clear trend with redshift in Fig. 6: high redshift clusters have lower early-type fractions than low redshift clusters. This result is not very sensitive to the details of the classifications. In those cases where clusters were classified by two different groups the fractions are very similar. The early-type fraction is much more stable from classifier to classifier than the ratio between the number of elliptical galaxies and the number of S0 galaxies (for discussions of the robustness of E/S0 fractions see Smail et al. 1997, Andreon 1998, Postman 1999, and Fabricant et al. 2000). This may not be surprising; as demonstrated by work on nearby galaxies the distinction between ellipticals and S0s is very difficult to make (e.g., Rix & White

1990, Jørgensen & Franx 1994).

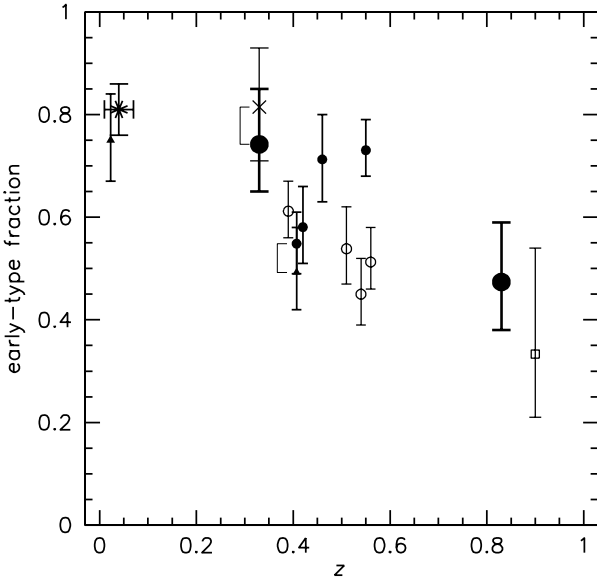


Fig. 6.— Evolution of the early-type fraction in rich clusters. The large symbols are CL1358+62 at  $z = 0.33$  and MS 1054-03 at  $z = 0.83$ . Sources of literature data are Andreon et al. (1997) (triangles), Dressler (1980) (star), Dressler et al. (1997) (small circles), and Lubin et al. (1998) (square). Filled symbols indicate clusters with  $L_x > 10^{44.5} h_{50}^{-2} \text{ ergs s}^{-1}$ . Two clusters (CL1358+62 at  $z = 0.33$  and CL0939+47 at  $z = 0.41$ ) have been classified twice, by independent groups; note the good agreement between these independent classifications (see text for details). The early-type fraction is a function of redshift: the early-type fraction at  $z = 0$  is roughly twice as large as the early-type fraction at  $z \sim 1$ .

The strong evolution of the early-type fraction implies that  $\sim 50\%$  of early-type galaxies in present-day rich clusters were either accreted onto the cluster or transformed from other galaxy types between  $z = 0$  and  $z = 1$ . Transformations (or a combination of transformations and accretion) are the most probable mechanism, because it is unlikely that the fraction of early-type galaxies among accreted galaxies exceeds the fraction of early-type galaxies among galaxies that are already in the cluster.

#### 4. MERGERS

One of the most surprising results of our survey is the high fraction of galaxies classified as “merger/peculiar” (van Dokkum et al. 1999). Thirteen out of 77 classified galaxies are mergers. F814W images of all mergers are shown in Fig. 7. The resolution of these images is  $0''.07 \text{ pixel}^{-1}$  (see Sect. B.2). The mergers display a variety of features. We find interacting pairs with distorted morphologies (e.g., 1340), double nuclei (e.g., 997) and galaxies with strong tidal features (e.g., 1760). Note that all mergers, including the interacting pairs and double nuclei, are counted as single objects.

The mergers are very luminous: the 13 mergers have a median luminosity  $M_B^T \approx -22$  ( $\sim 2L_*$  at  $z = 0.83$ ), and five of the sixteen most luminous cluster galaxies were classified as mergers. We calculated the luminosity of merging pairs by taking the sum of the luminosities of the individual merging galaxies. As argued in van Dokkum et al. (1999), the majority of the mergers will probably evolve into elliptical galaxies. The merger fraction in MS 1054 is comparable to the elliptical fraction: the number of elliptical galaxies “in formation” is similar to the number of elliptical galaxies already formed. Assuming the galaxy population in MS 1054-03 is typical for rich clusters at its redshift, this implies up to  $\sim 50\%$  of elliptical galaxies

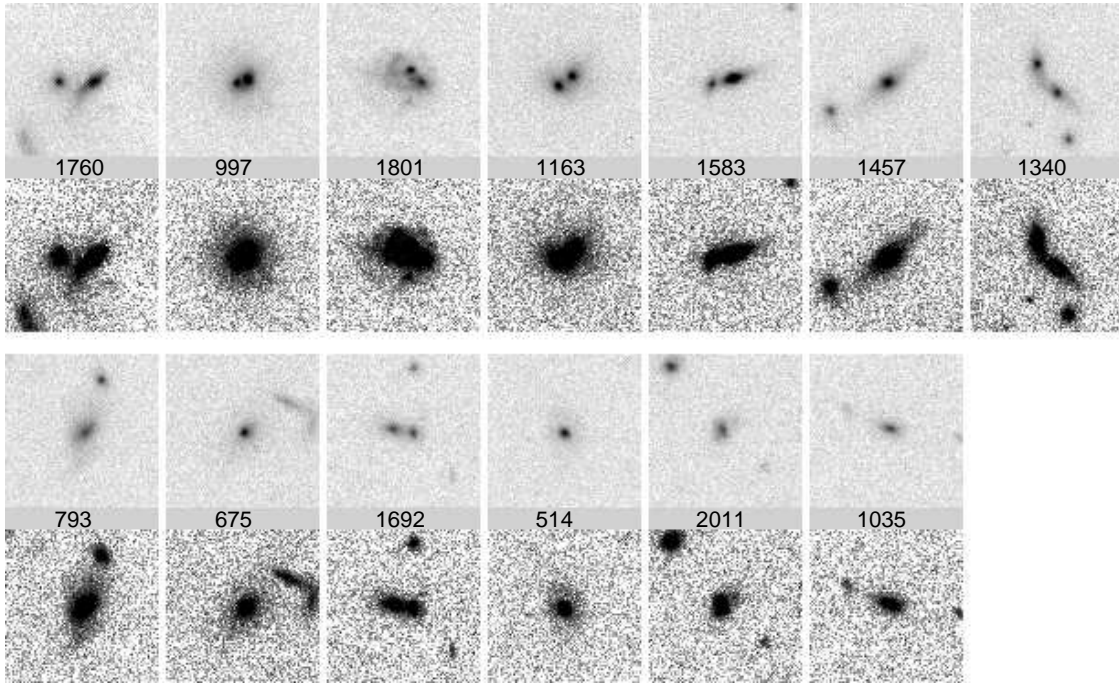


Fig. 7.— F814W images of the thirteen galaxies classified as “merger/peculiar”, displayed at two contrast levels. The mergers show a variety of features; we find double nuclei, tidal tails and/or interacting pairs with distorted morphologies. Note that all mergers are confirmed members of the cluster.

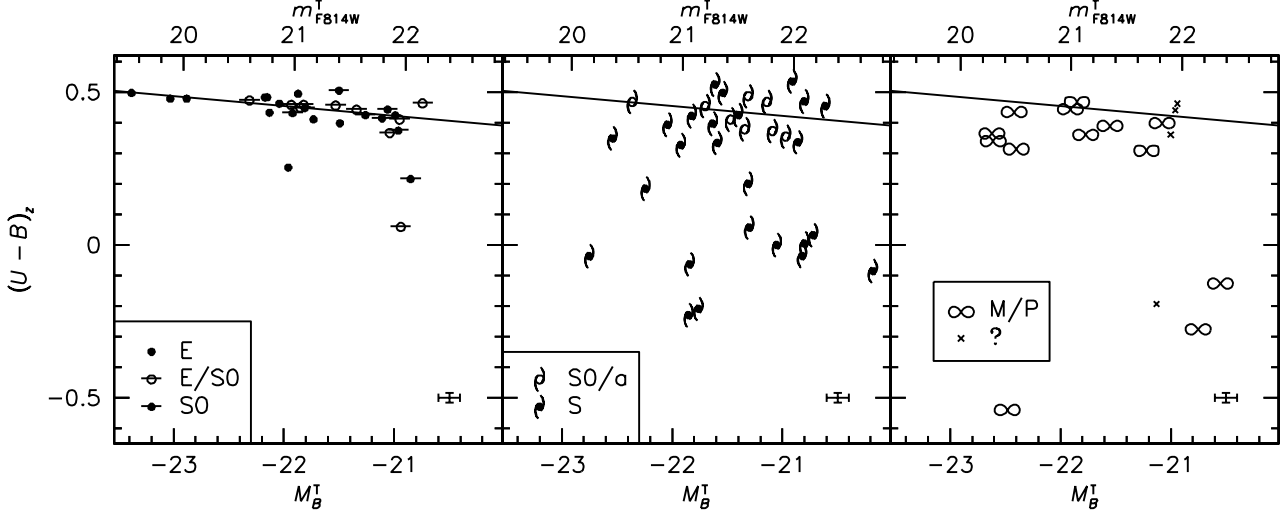


Fig. 8.— The restframe  $U - B$  versus  $B$  color-magnitude relation for different morphologies. There is a clear trend with morphology. Most early-type galaxies follow a tight and well-defined CM relation, although there are a few outliers. The drawn line in each plot is a fit to the CM relation of the early-type galaxies (Es, E/S0s, and S0s). Spiral galaxies have a large scatter, and are on average bluer than early-type galaxies in MS 1054–03. The mergers follow the same CM relation as the early-type galaxies, but are slightly offset to the blue and show a larger scatter.

formed in mergers at  $z < 1$  (see van Dokkum et al. 1999).

## 5. THE COLOR-MAGNITUDE RELATION AND THE BUTCHER-OEMLER EFFECT

### 5.1. The CM Relation for Different Morphologies

The color-magnitude relation for spectroscopically confirmed cluster members is shown in Fig. 8. There is a strong trend with morphology. Most early-type galaxies follow a tight and well defined relation, but there are three early-type galaxies which are fairly blue. Luminous blue early-type galaxies are very rare in clusters at lower redshift (e.g., van Dokkum et al. 1998a). The spiral galaxies have a much larger scatter in their colors than the early-type galaxies. As might be expected, some are very blue, but a fairly large number are quite red and lie close to the relation of the early-type galaxies. The mergers are only slightly bluer than the early-type galaxies, and follow a much tighter relation than the spiral galaxies.

We quantified these effects by determining the form of the CM relation from a fit to the early-type galaxies, and subtracting this fit from the observed relation. For each morphological subsample we then computed the offset and scatter in the CM relation from the distribution of residuals. The fitting procedure minimizes the scatter in the residuals, computed using the biweight statistic (Beers et al. 1990). The biweight gives low weight to outliers, and was also used in the studies of van Dokkum et al. (1998a) and Stanford et al. (1998). The fit to the early-type galaxies (Es, E/S0s, and S0s) has the form

$$(U - B)_z = -0.032(M_B^T + 22) + 0.454. \quad (1)$$

Note that no early-type galaxies were excluded from the fit. We tested the sensitivity of our results to the fitting procedure by comparing the biweight minimalisation to a least squares fit excluding the three bluest early-type galaxies. The least squares fit has the form  $(U - B)_z = -0.030(M_B^T + 22) + 0.456$ , and gives very similar results for the scatter of the CM relation as the biweight fit. The predicted colors from the CM relation were subtracted from the observed colors. For each morphological

subsample the mean and scatter in the distribution of residuals  $\Delta(U - B)_z$  were computed using the biweight statistic. Uncertainties in the scatter were determined from bootstrap resampling. The results are listed in Table 3.

The observed scatter in the early-type galaxies is low at  $0.029 \pm 0.005$ . The intrinsic scatter is  $0.024 \pm 0.006$ . This scatter is much smaller than that of the full sample ( $0.081 \pm 0.026$ ). The sample of early-type galaxies is too small to divide it into smaller subsamples.

From Table 3 we can see that the spiral galaxies and mergers are more heterogeneous in their colors than the early-type galaxies, with the spirals showing the largest scatter. On average the spiral galaxies are much bluer than the early-type galaxies, but not all of them are blue: in fact, only 12 out of 26 spiral galaxies and none of the SO/a galaxies are more than 0.2 magnitudes bluer than the CM relation. The mergers seem to follow the same CM relation as the early-type galaxies, but are slightly offset to the blue and show a larger scatter. The average offset between the CM relation of the early-type galaxies and the mergers is  $-0.07 \pm 0.02$  magnitudes. The scatter in the CM relation of the mergers is  $0.07 \pm 0.04$ , more than twice as large as the scatter of the early-type galaxies, and comparable to the mean offset from the CM relation.

### 5.2. Radial Dependence of the Color-Magnitude Relation

In the cluster CL 1358+62 at  $z = 0.33$ , the scatter and offset of the color-magnitude relation are dependent on  $R$ , the projected distance to the BCG; S0 galaxies in the outer parts of CL 1358+62 have a larger scatter in the CM relation and a bluer mean color than S0 galaxies in the inner parts (van Dokkum et al. 1998a). If this trend is caused by an age gradient in the cluster one might expect it to strengthen at higher redshift. In Fig. 9 the residuals from the CM relation are plotted against  $R$ . There is no significant correlation between  $\Delta(U - B)_z$  and  $R$  for the early-type galaxies. The trend observed in CL 1358+62 is indicated by the broken line in Fig. 9; our data are not of sufficient quality to detect or rule out such a trend in MS 1054–03.

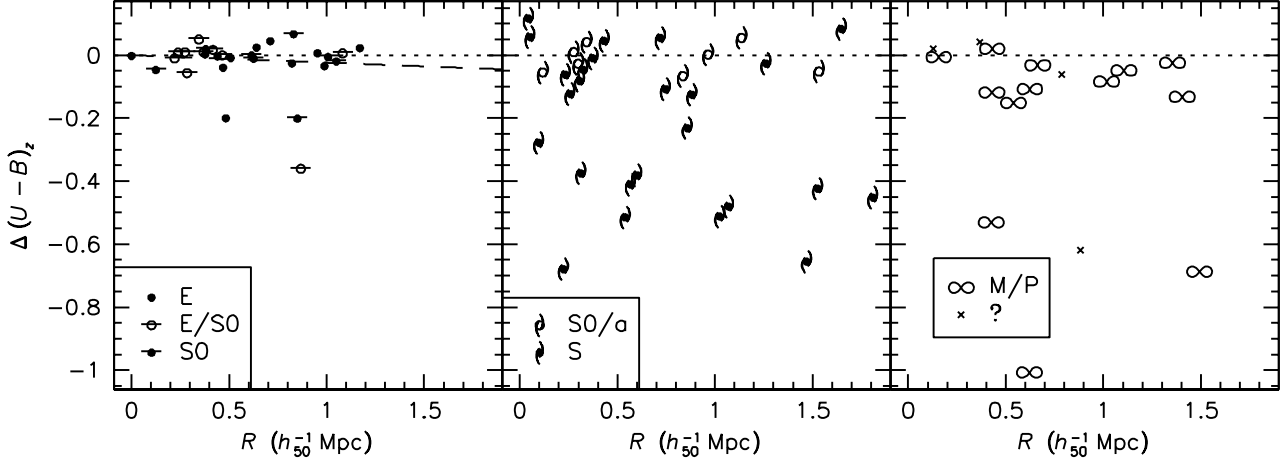


Fig. 9.— Residual from the color-magnitude relation plotted against  $R$ , the projected distance from the BCG. The dashed line indicates the trend found in the CM relation of S0 galaxies in the cluster CL 1358+62 at  $z = 0.33$ . There is no significant correlation between  $(U-B)_z$  and  $R$  for the early-type galaxies, although we cannot exclude a similar trend as in CL 1358+62. Note the absence of early-type galaxies at  $R > 1.2 h_50^{-1} \text{ Mpc}$ .

We note that there seems to be a larger fraction of red spiral galaxies in the core of the cluster than at larger radii, although the numbers are small. Only three out of eleven spiral galaxies at  $R < 0.5 h_50^{-1} \text{ Mpc}$  are more than 0.2 magnitudes bluer than the CM relation, compared to nine out of fifteen at  $R > 0.5 h_50^{-1} \text{ Mpc}$ .

### 5.3. The Butcher-Oemler Effect

There have been very few attempts to extend measurements of the Butcher & Oemler (1978a, 1984) effect beyond  $z \sim 0.5$ , partly because field contamination is more severe at higher redshift. Here, we use our extensive dataset on MS 1054-03 to measure the Butcher-Oemler effect in a cluster at  $z = 0.83$ .

Butcher & Oemler (1984) defined the blue fraction as the fraction of the cluster population within  $R = R_{30}$  that is more than 0.2 magnitudes bluer in restframe  $B - V$  than the ridge line of the CM relation, with  $R_{30}$  the radius of a circular aperture containing 30% of the cluster galaxies (Butcher & Oemler 1984). They also imposed a fixed magnitude cutoff of  $M_V < -20$  in the restframe. Note that this procedure ignores luminosity evolution.

The value of  $R_{30}$  can be determined from the projected surface density profile of the cluster (cf. Butcher & Oemler 1978b). We determine the surface density profile of MS 1054-03 from our sample of spectroscopically confirmed members, after correcting for incompleteness (see Sect. 2.1.2). Butcher & Oemler (1984) used unpublished models by Aarseth to extrapolate the observed surface density profile to large radii. At large radii, these models are well approximated by a power law (see Butcher & Oemler 1978b). From a power law fit to the observed surface density profile of MS 1054-03 we find  $\approx 20\%$  of its galaxy population is outside the field of our spectroscopic survey. We find  $R_{30} = 49''$ , and a concentration index  $C \equiv \log(R_{60}/R_{20}) = 0.53$ . We conclude that MS 1054-03 is a compact cluster according to the Butcher & Oemler (1984) criterion.

To test the robustness of our approach we also determine the surface density profile from red galaxies in the HST mosaic, by selecting all galaxies to  $I_{F814W} = 24$  whose colors are within  $\pm 0.2$  magnitudes of the color-magnitude relation. This surface density profile, extended by a power law fit, gives  $R_{30} = 59''$ . In the following, we take  $R_{30} = 0.5 h_50^{-1} \text{ Mpc}$  (equivalent to 53'').

This number is very similar to values measured by Butcher & Oemler (1984) for clusters at lower redshift.

We correct our spectroscopic sample for incompleteness by assigning each galaxy a weight equal to the inverse of the magnitude selection function (cf. Sect. 2.1.2). The corrected number of cluster galaxies with  $I_{F814W} \leq 22.5$  and  $R < R_{30}$  is 67. Eleven (16%) are blue according to the Butcher & Oemler criterion, where we have converted restframe  $U - B$  to  $B - V$  using  $\Delta(U - B) = 1.4\Delta(B - V)$ , as derived from models by Worthey (1994).

Our spectroscopic sample extends to  $I_{F814W} \approx 22.5$ . The magnitude limit that is equivalent to the Butcher & Oemler limit of  $M_V = -20$  in the restframe is  $I_{F814W} \sim 24$ , where we have used Eq. B3, and  $B - V = 1$  in the restframe. To determine the number of blue galaxies with  $22.5 < I_{F814W} < 24$  we cannot use our sample of confirmed members, and hence we used the full photometric dataset, and applied a correction for field contamination. We predict the number of field galaxies in this magnitude range by fitting a power law to the differential galaxy counts at  $20 < I < 22.5$ . These counts were determined from our sample of confirmed field galaxies, and corrected for incompleteness. The power law fit has exponent  $\alpha_I = 0.33$ , similar to values determined from deep photometric surveys (e.g., Smail et al. 1995). Of 115 galaxies with  $22.5 < I_{F814W} < 24$  and  $R < R_{30}$ , 27 are predicted to be field galaxies. Assuming the color distribution of the field galaxies is identical to that of field galaxies in our spectroscopic sample, we find 23 of 88 cluster galaxies with  $22.5 < I_{F814W} < 24$  and  $R < R_{30}$  are blue.

Combining these numbers with those determined from the spectroscopic sample, we find a Butcher & Oemler blue fraction  $f_B = 0.22$ , with a random error of  $\pm 0.04$ . From experimenting with the value of  $R_{30}$ , the completeness corrections, and the field correction we estimate the systematic uncertainty is  $\pm 0.03$ . Assuming the random error and the systematic error can be added in quadrature, we find  $f_B = 0.22 \pm 0.05$ .

Figure 10 shows the redshift evolution of the fraction of blue galaxies in rich clusters. The blue fraction in MS 1054-03 is similar to typical blue fractions in optically selected clusters at  $z \sim 0.4$ , and higher than typical blue fractions in X-ray selected clusters at  $z \sim 0.2$ . The extremely high fractions of blue galaxies found by Rakos & Schombert (1995) in clusters at  $z > 0.5$

( $f_B \sim 0.8$  at  $z \sim 0.8$ ) are not confirmed here. This may in large part be due to differences in procedure: Rakos & Schombert (1995) did not impose a strict radial limit, and determined blue fractions by comparing the colors of galaxies in their high redshift clusters to those of present-day elliptical galaxies. This method does not take passive evolution of the ridge-line of the CM relation into account.

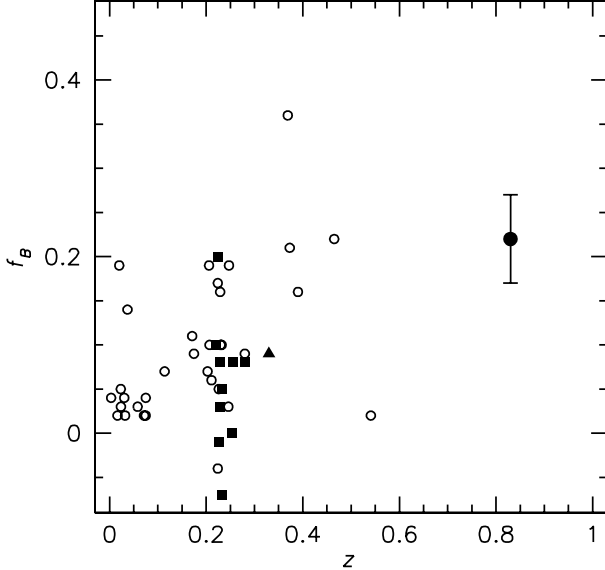


Fig. 10.— The evolution of the Butcher-Oemler blue fraction with redshift. The large symbol at  $z = 0.83$  is MS 1054-03. Circles are clusters from Butcher & Oemler (1984), squares are clusters from Smail et al. (1998), and the triangle is CL 1358+62 from Fabricant et al. (1991). For clarity no errorbars are shown on the datapoints from the literature; typical errors are  $\sim 0.03$  for low redshift clusters and  $\sim 0.08$  for intermediate redshift clusters. Filled symbols are X-ray selected clusters. The blue fraction in MS 1054-03 does not exceed typical values for clusters at  $z \sim 0.4$ .

We note that three of the four spectroscopically confirmed blue galaxies within  $R_{30}$  (galaxies 1422, 1459 and 1650) are late-type spiral galaxies; the eight other spiral galaxies with  $R < R_{30}$  are red. One blue galaxy (1035) is classified as merger. Spectroscopically, 1035 and 1650 are E+A galaxies, galaxy 1459 has strong H $\delta$  absorption and weak [O II] 3727 Å emission, and galaxy 1422 has an early-type spectrum.

## 6. EVOLUTION OF THE COLOR-MAGNITUDE RELATION OF EARLY-TYPE GALAXIES FROM $Z = 0$ TO $Z = 1$

### 6.1. Evolution of the Slope

The slope and scatter of the CM relation of early-type galaxies can be compared to data at lower redshift. Fig. 11 shows the evolution of the slope of the CM relation as a function of redshift. Data points are from Bower et al. (1992) for the Coma cluster, van Dokkum et al. (1998a) for CL 1358+62 at  $z = 0.33$ , and Ellis et al. (1997) for three clusters at  $z \approx 0.55$ . We have used the Worthey (1994) models to transform  $U - V$  (Bower et al. 1992) and Ellis et al. 1997) and  $B - V$  colors (van Dokkum et al. 1998a) to  $U - B$  colors. For solar metallicity these models give  $\Delta(U - B) = 1.4\Delta(B - V)$  and  $\Delta(U - B) = 0.6\Delta(U - V)$ .

The samples of Bower et al. (1992) and Ellis et al. (1997) only cover the inner parts of the clusters. Furthermore, in these studies colors were measured inside fixed apertures of

$10 h_{50}^{-1}$  kpc rather than within effective radii. For CL 1358+62 and MS 1054-03 we determined the slope for the inner parts of the cluster as well as for the whole sample. To enable a direct comparison to Bower et al. (1992) and Ellis et al. (1997) we also determined the slope of the CM relation in the inner parts of the cluster with color measurements in a fixed aperture of  $10 h_{50}^{-1}$  kpc.

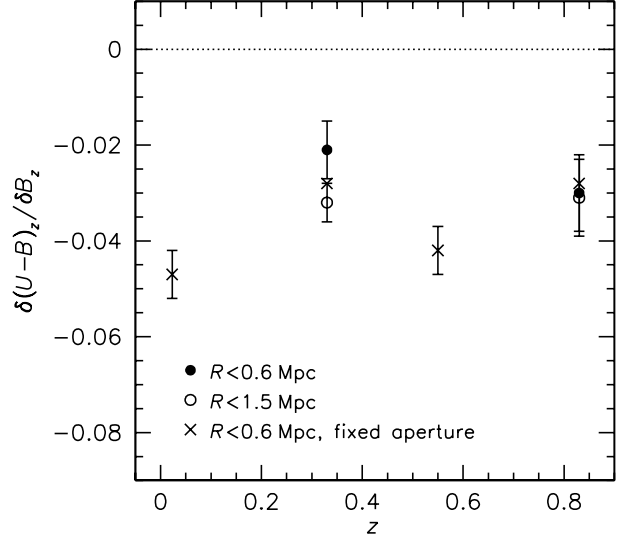


Fig. 11.— Evolution of the slope of the CM relation of early-type galaxies, based on HST photometry. In order of increasing redshift the data points are from Bower et al. ( $z = 0.023$ ), van Dokkum et al. (1998a) ( $z = 0.33$ ), Ellis et al. (1997) ( $z = 0.55$ ), and this study ( $z = 0.83$ ). The data are consistent with a constant slope with redshift.

A linear fit to the evolution of the slope in the inner parts of the clusters gives  $\delta(U - B)_z / \delta B_z = (0.013 \pm 0.016)z - (0.041 \pm 0.008)$ . We conclude that there is no evidence that the slope of the CM relation depends on redshift. If the slope in the relation at  $z = 0$  is (partly) due to a systematic age gradient, such that high luminosity galaxies have higher luminosity weighted ages than low luminosity galaxies, one might expect the slope to become steeper at higher redshift (e.g., Kodama et al. 1998). We see no such effect in the data presented here. This result is in agreement with the studies of Stanford et al. (1998) and Kodama et al. (1998), who used ground based photometry and HST morphologies to determine the slope and scatter of the CM relation of early-type galaxies in clusters at  $0 < z < 1$ .

### 6.2. Evolution of the Scatter: the Progenitor Bias

The evolution of the scatter in the CM relation of early-type galaxies is shown in Fig. 12. Solid symbols are from the same sources as in Fig. 11, and are based on WFPC2 colors (except for the Coma cluster at  $z = 0.02$ ). Open symbols are taken from Stanford et al. (1998), and are based on ground based photometry. Stanford et al. (1998) assumed their “blue – red” colors are close to restframe  $U - V$ , and we transformed their measurements using  $\Delta(U - B) = 0.6\Delta(\text{blue} - \text{red})$ .

The scatter in the CM relation of early-type galaxies is low at all redshifts, consistent with the results of Stanford et al. (1998). In particular, the scatter at  $z = 0.83$  is almost identical to the scatter at  $z = 0$ . This may seem remarkable, because the scatter in the CM relation might be expected to increase with redshift due to increasing fractional age differences between galaxies

(see, e.g., Bower et al. 1992, van Dokkum et al. 1998a, Ferreras & Silk 2000). The underlying assumption of this argument is that early-type galaxies are drawn from the same sample at high and low redshift, and that they evolve in a regular way between  $z = 1$  and  $z = 0$ . However, the low early-type fraction and the presence of the mergers demonstrate that the sample of early-type galaxies in MS 1054–03 only forms a subset of the population of present-day early-type galaxies.

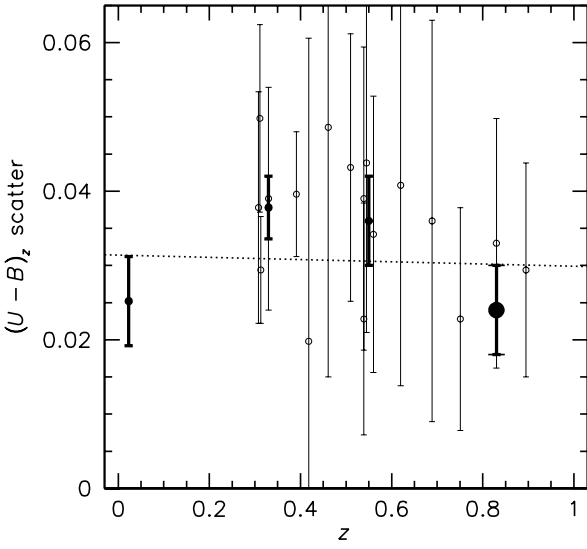


Fig. 12.— Evolution of the scatter in the CM relation of early-type galaxies. Filled data points are from the same sources as those in Fig. 11, and are based on HST photometry (except the Coma cluster). Open data points are from Stanford et al. (1998) and are based on ground based colors. Note that the HST measurements have smaller uncertainties than the ground based measurements. The broken line is a linear least squares fit to the HST photometry. The data are consistent with a constant scatter with redshift.

Figure 13 shows the scatter in the CM relation of *all* known progenitors of present-day early-type galaxies. Specifically, this includes the mergers in MS 1054–03 since they will probably evolve into early-type galaxies. The intrinsic scatter in the combined sample of mergers and early-type galaxies in MS 1054–03 is twice as high as the scatter in the early-type galaxies alone, and the data indicate an increase in the scatter by a factor two between  $z = 0$  and  $z = 1$ . We fitted linear relations to the data shown in Fig. 12 and Fig. 13. These fits are indicated by broken lines. The best fitting relation changes from a constant to substantial evolution.

We note that in addition to the mergers a fraction of the spiral galaxies in MS 1054–03 may also evolve into early-type galaxies (e.g., Dressler et al. 1997). It is very hard to establish which, if any, of the spiral galaxies in MS 1054–03 are destined to become S0 galaxies. If the mergers and all red spiral galaxies (i.e., those within 0.2 magnitudes of the CM relation) evolve into early-type galaxies, the scatter in the color-magnitude relation of all progenitors of present-day early-type galaxies is  $\approx 0.063$  at  $z = 0.83$ .

These results show that the properties of samples of early-type galaxies in distant clusters are different from the properties of the full sample of progenitors of present-day early-type galaxies. Distant early-type galaxies are the progenitors of the oldest present-day early-type galaxies. This “progenitor bias”

can lead to biased age estimates. As demonstrated here, the scatter in the color-magnitude relation is particularly sensitive to this bias. In a forthcoming paper we model the redshift evolution of the scatter in the CM relation, taking morphological evolution into account.

An open question is whether the galaxy population in MS 1054–03 is typical for its redshift. The cluster is young and still forming, and the high merger fraction could be related to this process (van Dokkum et al. 1999). If this is the case, this epoch of enhanced merging could occur at different redshifts for different clusters.

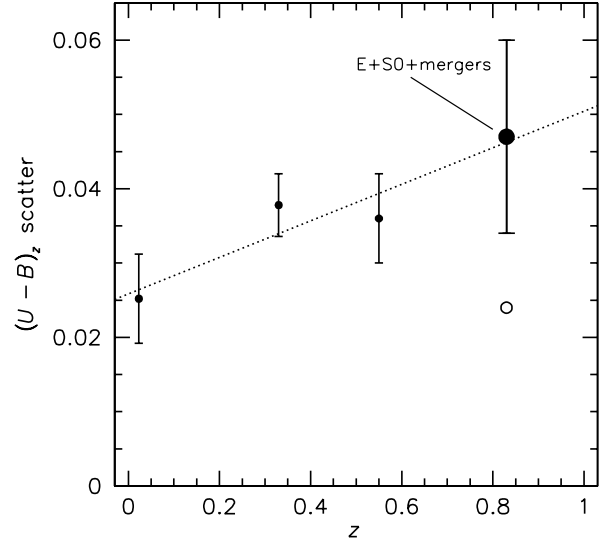


Fig. 13.— Evolution of the scatter in the CM relation of all progenitors of present-day early-type galaxies. This includes the mergers in MS 1054–03 at  $z = 0.83$ . For comparison, the open symbol at  $z = 0.83$  shows the scatter of the early-type galaxies alone. The points at lower redshift are identical to those in Fig. 12. The broken line is a linear least squares fit to the data. The scatter in the full sample of progenitors of present-day early-type galaxies increases by a factor  $\sim 2$  between  $z = 0$  and  $z = 1$ .

## 7. SUMMARY AND CONCLUSIONS

We have presented a study of the galaxy population in the rich cluster MS 1054–03 at  $z = 0.83$ . Our sample of 81  $I$ -band selected galaxies is currently the largest sample of confirmed cluster galaxies at  $z > 0.5$  observed with HST. One of the most striking results of our survey of MS 1054–03 is the high fraction of mergers among the  $L > L_*$  cluster population (van Dokkum et al. 1999). In the present paper we focussed on the early-type fraction, the Butcher-Oemler effect, and the color-magnitude relation in MS 1054–03.

The early-type fraction in MS 1054–03 is much lower than that in rich clusters at intermediate and low redshift. Combining our data with data from the literature we find a continuous decrease in the early-type fraction with redshift. The early-type fraction changes by a factor  $\sim 2$  from  $z = 0$  to  $z = 0.83$ . This result is robust and independent of the classification procedure. It is reasonable to assume that the mergers in MS 1054–03 will evolve into early-type galaxies. This implies that the early-type fraction in this cluster will increase from 44 % to 61 % in approximately 1 Gyr.

MS 1054–03 displays a similar Butcher-Oemler effect as

clusters at intermediate redshift:  $f_B = 0.22 \pm 0.05$ . This may appear to be at variance with the low early-type fraction, but is a result of the fact that most spiral galaxies are red, similar to spiral galaxies in nearby clusters (e.g., Butcher & Oemler 1984). Of eleven spiral galaxies within  $R = R_{30}$ , only three are blue. The blue fraction in MS 1054–03 is much lower than values reported by Rakos & Schombert (1995) for clusters at  $z > 0.6$ . This is probably due to the fact that these authors used a different procedure to measure the blue fraction.

We studied the CM relation as a function of morphology. The early-type galaxies follow a remarkably tight and well defined relation, with an observed scatter of  $0.029 \pm 0.005$  in restframe  $U - B$ . There is no significant dependence of the CM relation of early-type galaxies on radius in the cluster; our small sample precludes us from confirming or ruling out a similar trend as found for S0 galaxies in the cluster CL 1358+62 at  $z = 0.33$  (van Dokkum et al. 1998a). The spiral galaxies exhibit a large range in their colors; they are offset to the blue by 0.22 magnitudes with respect to the CM relation of the early-type galaxies, but many are as red as early-type galaxies of the same luminosity. This could be due to a spread in age, metallicity, and/or dust content.

The mergers are only slightly bluer than the early-type galaxies, by  $0.07 \pm 0.02$  magnitudes. The scatter in their CM relation is  $0.07 \pm 0.04$ . Only three of the thirteen mergers are more than 0.2 magnitudes bluer than the CM relation; these are the only mergers with detected [O II] 3727 Å emission. It may appear surprising that the mergers are so red; mergers in the nearby Universe are typically blue and have high star formation rates (Liu & Kennicutt 1995). However, most of the spiral galaxies in MS 1054–03 are red as well, and the red colors of the mergers are probably a result of the environment: galaxies in and near a rich cluster are likely redder than typical field galaxies. A quantitative demonstration of this effect is that the median color of

the mergers ( $\langle U - B \rangle_z = 0.36$ ) is very similar to the median color of the full sample of cluster galaxies ( $\langle U - B \rangle_z = 0.41$ ).

The slope and scatter of the CM relation of the early-type galaxies in MS 1054–03 are very similar to those of clusters at lower redshift, confirming previous studies. However, the presence of the mergers and the low early-type fraction in MS 1054–03 demonstrate that early-type galaxies in distant clusters are a biased set, and not representative of the full sample of progenitors of present-day early-type galaxies. This “progenitor bias” has a large effect on the scatter in the color-magnitude relation: the scatter in the full sample of all progenitors of present-day early-type galaxies (i.e., including the mergers in MS 1054–03) shows strong evolution with redshift. The scatter increases by a factor  $\sim 2$  between  $z = 0$  and  $z = 1$ . The main uncertainty in this result is the assumption that the galaxy population in MS 1054–03 is typical for its redshift.

It is clearly important to extend this type of analysis to other clusters, and to higher redshift. Of particular interest is the evolution of the early-type fraction, since it may be a fairly robust measure of morphological evolution. The large format of the HST imaging was very important in our study, because the mergers typically reside at large radii (van Dokkum et al. 1999), and it allowed efficient spectroscopic follow-up. This study demonstrates that the combination of extensive spectroscopy and large format, high resolution imaging can provide important insights into the assembly and evolution of cluster galaxies.

We thank the anonymous referee for constructive and valuable comments, which improved the paper significantly. We thank G. Luppino for providing us with a ground based  $R$  band image of MS 1054–03. We appreciate the help of the staff of the W. M. Keck Observatory. Support from STScI grant GO07372.01-96A is gratefully acknowledged.

## APPENDIX

### DETAILS OF THE SPECTROSCOPIC SURVEY

#### *Reduction*

The reduction involved bias subtraction, flatfielding, removal of cosmic rays, rectification, and sky subtraction. Critical steps in the reduction process were flatfielding and cosmic ray removal. Flatfielding is difficult because the Tektronix CCD has severe fringing at  $\lambda \gtrsim 7500$  Å. The fringes have characteristic scales of  $\lambda \sim 20$  Å, and amplitudes to  $\sim 8\%$ . The signal-to-noise in the sky subtracted spectra critically depends on the success of removing the fringe pattern. For this reason we took flatfield exposures at a range of hour angles and grating angle settings, bracketing the hour angle and grating angle setting at the time of the observations. The flatfields that produced the lowest noise in the sky lines were used. This procedure reduced the amplitude of the fringes to  $\approx 0.5\%$ .

Cosmic rays were removed as described by van Dokkum & Franx (1996). The galaxy spectra and sky lines were fitted with appropriate functions and subtracted. Pixels that deviated significantly from the expected noise in the subtracted functions were flagged as possible cosmic rays. Several slits in the masks were tilted in order to cover more than one object with the same slit. Such tilted slits produce tilted sky lines in the 2D spectra, and these were not adequately removed by the fitting functions. Residuals from sky lines in these slits were removed interactively. After subtraction of the cosmic rays, the frames were carefully checked by eye to ensure that only cosmic rays were removed.

For each row in each slit a wavelength solution was obtained from the sky lines. Wavelengths of unblended lines (the [O I] 5577, 6300 Å lines and the OH P1 lines) were taken from the Osterbrock et al. (1996) catalog. The 2D galaxy spectra were corrected for the S-distortion and transformed to a common wavelength scale. Sky spectra were determined from the edges of each slit, and subtracted. Finally, 1D spectra were extracted from the 2D spectra using APSUM in IRAF.

#### *Determination of Spectral Types*

We have measured equivalent widths of the [O II] 3727 Å emission line and the H $\delta$  4102 Å Balmer line. The strength of the [O II] line is a measure of ongoing star formation, and the strength of the H $\delta$  line is sensitive to recent star formation activity (e.g., Barbaro & Poggianti 1997). We used the line strength index definitions of Fisher et al. (1998). Line strengths are positive if the line is in

absorption, and negative if in emission. The restframe equivalent widths and their associated errors are listed in Table 1. For most galaxies the errors are a few Angstroms.

Spectral types were assigned to the galaxies based on the strengths of [O II] and H $\delta$ . The definitions of the spectral types are also analogous to those of Fisher et al. (1998). The spectral types are “absorption”, “emission”, and “E+A” (Dressler & Gunn 1983). Emission line galaxies have [O II] 3727 Å emission line strength greater than 5 Å. Galaxies with [O II] emission line strength less than 5 Å and Balmer absorption line strength greater than 4 Å are classified as “E+A” galaxies. Galaxies lacking significant [O II] emission and strong H $\delta$  absorption have spectral type “absorption”. The spectral types are listed in Table 1. Spectral types which within  $1\sigma$  of another type (as determined from the errors in [O II] and H $\delta$ ) are labeled with a question mark.

## REDUCTION OF WFPC2 DATA AND PHOTOMETRY

### *Observations and Initial Reduction*

The MS 1054–03 field was observed with the F606W and F814W filters on 1998 May 30. We obtained a mosaic of six slightly overlapping pointings. Six exposures were taken in each filter and at each position, giving a total of 72 exposures. In order to improve the sampling the six exposures at each position were split in two sets of three, with relative offsets between the sets of 5.5 pixels in  $x$  and  $y$ . Furthermore, the three exposures in each set were shifted relative to each other by  $\pm 3.0$  pixels, to facilitate the identification of hot pixels. Total exposure times were 6500 s in each filter for each pointing. The layout of the field is shown in Fig. 4.

The pipeline reduction was performed at the Space Telescope Science Institute. Further processing involved masking of bad pixels and bad columns, shifting the exposures to a common position on the sky, sky subtraction, identifying cosmic rays and hot pixels, and combining the images. The most labour intensive step in this process is the cosmic ray removal. We experimented with the CRREJECT task in the STSDAS package, but found that the quality of the combined image is quite sensitive to the choice of input parameters. In particular, the noise in the final combined image can be higher than expected from the noise in the individual input images. We therefore followed a different strategy. We compared the exposures with integer pixel shifts in each set of three, and removed cosmic rays in several steps. First, the expected noise  $\sigma_{\text{exp}}$  in each pixel was calculated from the minimum of the three exposures. Then, the task GCOMBINE in IRAF was used to identify cosmic rays, with  $\sigma_{\text{exp}}$  as the input noise model. The output of GCOMBINE is a cosmic ray cleaned average of the three exposures, an image containing the number of cosmic rays found, and an output noise map  $\sigma_{\text{true}}$  based on the actual variation in each pixel. Finally, the noise model and the measured noise were compared to identify pixels affected by cosmic rays in two of the three exposures. The method proved to work very well. In particular, in no cases were the central pixels of stars or galaxies mistaken for cosmic rays. After identifying the cosmic rays each set of three exposures with integer pixel shifts was averaged, excluding the flagged pixels. As a result there are two reduced images of each field and in each filter, shifted with respect to each other by 5.5 pixels.

### *Combination of Interlaced Images*

As is well known, the  $0.^{\prime\prime}1 \times 0.^{\prime\prime}1$  WFC pixels undersample the HST WFPC2 PSF. The sampling can be improved by obtaining multiple exposures of the same field, offset by subpixel shifts. The shifted exposures can be “drizzled” on a finer grid (see Fruchter & Hook 1999 and references therein). If the offsets between the exposures are precisely 0.5 pixels, the images are interlaced. In this special case there is a one-to-one correspondence between pixels in the original image and in the higher resolution output image. The improvement in the sampling is a factor  $\sqrt{N}$ , with  $N = 2$  or  $N = 4$  the number of independent positions.

The present observations are taken at two independent positions, offset by  $\pm 5.5$  pixels. As illustrated in Fig. B14, these two exposures sample an  $(x, y)$  grid which is rotated by  $45^\circ$  with respect to the original grid. We combined the two offset exposures of each field by copying the pixels on a finer grid. The transformations from the offset input images  $I^A$  and  $I^B$  to the interlaced output image  $I^{AB}$  are

$$I_{n+i-j, i+j-1}^{AB} = I_{i,j}^A \quad (B1)$$

$$I_{n+i-j, i+j}^{AB} = I_{i,j}^B, \quad (B2)$$

with  $n \times n$  the size of the input images, and  $i, j = 1, 2, \dots, n$ . The output image has a size  $2n \times 2n$ . The area of the output image containing data is  $\sqrt{2}n \times \sqrt{2}n = 2n^2$  pixels. The pixel size is  $0.^{\prime\prime}1/\sqrt{2} = 0.^{\prime\prime}071$ .

### *Image Restoration*

Although the interlacing improved the sampling by a factor  $\sqrt{2}$ , the improvement in resolution is smaller. This is caused by the wings of the PSF, and the subpixel response function (e.g., Krist 1995). In order to correct the photometry for these effects the interlaced images were restored using CLEAN (Høgbom 1974). The CLEAN algorithm requires a model for the PSF. For all cluster galaxies subsampled PSFs appropriate for the positions of the galaxies on the WFC chips were created using Tiny Tim (Krist 1995), version 4b. The exposures were mimiced by creating a copy of each subsampled PSF and shifting it by  $0.^{\prime\prime}05$  in  $x$  and  $y$ . The PSFs were then rebinned to the WFC resolution, and convolved with the subpixel response function using the kernel given in Krist (1995). Finally, each PSF was combined with its  $0.^{\prime\prime}05$  shifted copy in the same way as the actual exposures. The effect of interlacing and subsequent CLEANING on noiseless data is demonstrated in Fig. B15. Note that most of the degradation of image A is caused by the coarse sampling of the PSF by the  $0.^{\prime\prime}1$  pixels.

### *Photometry*

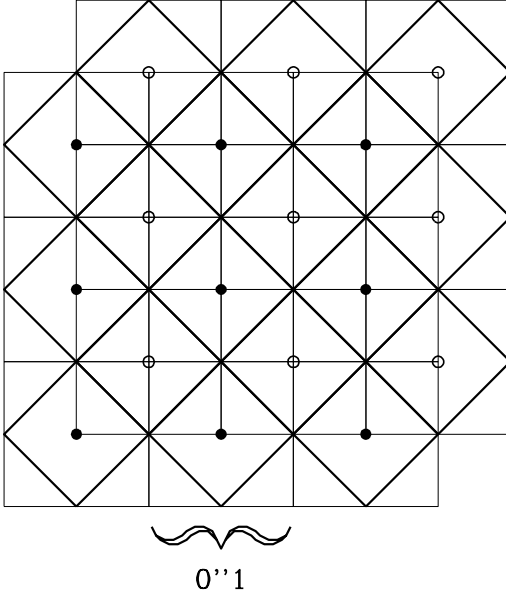


Fig. B14.— Illustration of interlacing using two independent positions. Solid circles are the centers of pixels in the first exposure, open circles are the centers of pixels in the second, offset, exposure. The solid circles and open circles sample a grid that is rotated by 45° with respect to the original grid. The output pixels are indicated by heavy lines. The output pixel size is  $0''.1/\sqrt{2}$ .

Figure B16 shows color images of the 81 spectroscopically confirmed cluster members in the HST WFPC2 mosaic. Total (“best”) magnitudes of these galaxies were determined from the HST data using the SExtractor program (Bertin & Arnouts 1996). Colors were determined from the HST data using PHOT in IRAF. The colors were measured within the effective radii of the galaxies, which were derived from fits of the galaxy images to  $r^{1/4}$  laws convolved with the PSF (see van Dokkum et al. 1998a). As explained in Sect. B.3 we used the CLEANed images for these measurements.

The observed F606W and F814W bands roughly correspond to restframe  $U$  and  $B$  for objects redshifted to  $z = 0.83$ . Following the method outlined in van Dokkum & Franx (1996) transformations were computed from the observed bands to redshifted  $B$  (denoted  $B_z$ ), and  $(U - B)_z$  colors:

$$B_z = F814W - 0.03(F606W - F814W) + 1.23 \quad (B3)$$

$$(U - B)_z = 0.76(F606W - F814W) - 1.14. \quad (B4)$$

The zero points of the F814W and F606W filters are taken from the HST Data Handbook (STScI, Baltimore). Total  $B_z$  magnitudes were converted to total absolute  $M_B^T$  magnitudes using  $H_0 = 50 \text{ km s}^{-1} \text{ Mpc}^{-1}$  and  $q_0 = 0.15$ .

The photometric accuracy can be assessed empirically, by comparing the two independent measurements of colors of objects in the overlapping regions between the six HST pointings. Note that this procedure limits the effects resulting from uncertainties in the CTE degradation of the WFPC2 chips. From this comparison we find that the average photometric uncertainty in the color is 0.016 for a single measurement. In our analysis of the scatter in the CM relation, this number is subtracted in quadrature from the measured scatter.

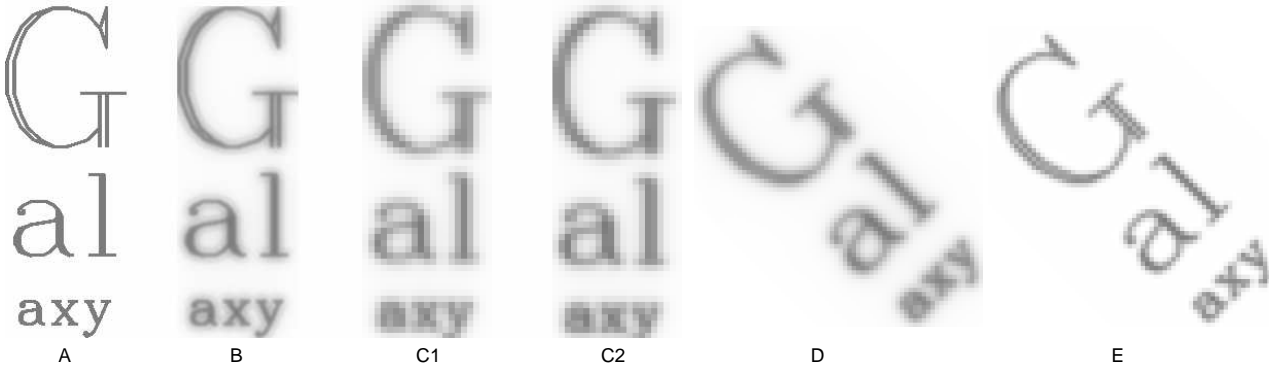


Fig. B15.— Effect of resolution enhancement as a result of interlacing and subsequent CLEANing. **A:** Original (“true”) image of dimensions  $2''.1 \times 5''.5$ ; **B:** image A convolved with HST WFPC2 PSF; **C1, C2:** image B sampled at WFPC2  $0''.1$  resolution and convolved with the subpixel response function, at two positions with relative offsets of  $0''.05$  in  $x$  and  $y$ . Note that most of the degradation of image A is a result of the coarse sampling. **D:** Interlaced combination of images C1 and C2, at  $0''.071$  resolution; **E:** CLEAN restoration of image D.

Figure available from  
<http://astro.caltech.edu/~pgd/cm1054/fig16.eps.gz>

Fig. B16.— Color images of the 42 most luminous spectroscopically confirmed cluster members in MS 1054–03. The images are created from the F606W and F814W exposures, and are sorted by total F814W magnitude. Each image is  $5.^{\prime\prime}9 \times 5.^{\prime\prime}9$ ; at the distance of MS 1054–03, this corresponds to  $63 \times 63 h_{50}^{-1}$  kpc. Note the large fraction of mergers among the most luminous galaxies in the cluster, and their fairly red colors.

## REFERENCES

Abadi, M. G., Moore, B. & Bower, R. G. 1999, MNRAS, 308, 947

Andreon, S., Davoust, E., & Heim, T. 1997, A&A, 323, 337

Andreon, S. 1998, ApJ, 501, 533

Aragon-Salamanca, A., Ellis, R. S., Couch, W. J., & Carter, D. 1993, MNRAS, 262, 764

Balogh, M. L., Schade, D., Morris, S. L., Yee, H. K. C., Carlberg, R. G., & Ellingson, E. 1998, ApJ, 504, L75

Barbaro, G., & Poggianti, B. M. 1997, A&A, 324, 490

Beers, T. C., Flynn, K., & Gebhardt, K. 1990, AJ, 100, 32

Bender, R., Saglia, R. P., Ziegler, B., Belloni, P., Gregg, L., Hopp, U., & Bruzual, G. 1998, ApJ, 493, 529

Bertin, E., & Arnouts, S. 1996, A&AS, 117, 393

Bower, R. G., Lucey, J. R., & Ellis, R. S. 1992, MNRAS, 254, 601

Butcher, H., & Oemler, A. 1978a, ApJ, 219, 18

Butcher, H., & Oemler, A., Jr. 1978b, ApJ, 226, 559

Butcher, H., & Oemler, A. 1984, ApJ, 285, 426

Couch, W. J., & Sharples, R. M. 1987, MNRAS, 229, 423

Couch, W. J., Barger, A. J., Smail, I., Ellis, R. S. & Sharples, R. M. 1998, ApJ, 497, 188

de Theije, P. A. M., & Katgert, P. 1999, A&A, 341, 371

Donahue, M., Voit, G. M., Gioia, I., Lupino, G., Hughes, J. P., & Stocke, J. T. 1998, ApJ, 502, 550

Dressler, A. 1980, ApJ, 236, 351

Dressler, A., & Gunn, J. E. 1983, ApJ, 270, 7

Dressler, A., Oemler, A., Jr., Couch, W. J., Smail, I., Ellis, R. S., Barger, A., Butcher, H., Poggianti, B. M., & Sharples, R. M. 1997, ApJ, 490, 577

Ellis, R. S., Smail, I., Dressler, A., Couch, W. J., Oemler, A., Jr., Butcher, H., & Sharples, R. M. 1997, ApJ, 483, 582

Fabricant, D. G., McClintock, J. E., & Bautz, M. W. 1991, ApJ, 381, 33

Fabricant, D., Franx, M., & van Dokkum, P. G. 2000, ApJ, submitted

Ferreras, I., & Silk, J. 2000, ApJ, in press (astro-ph/9910385)

Fisher, D., Fabricant, D., Franx, M., & van Dokkum, P. G. 1998, ApJ, 498, 195

Franx, M., & van Dokkum, P. G. 1996, in New Light on Galaxy Evolution (IAU 171), R. Bender & R. L. Davies, Eds., Kluwer, p. 233

Fried, J. W. 1988, A&A, 189, 42

Fruchter, A. S., Hook, R. N. 1999, preprint (astro-ph/9808087)

Gunn, J. E. & Gott, J. R., III 1972, ApJ, 176, 1

Hoekstra, H., Franx, M., & Kuijken, K. 2000, ApJ, in press (astro-ph/9910487)

Høgbom, J. A. 1974, A&AS, 15, 417

Jansen, R. A., Franx, M., Fabricant, D., & Caldwell, N. 2000, ApJS, in press (astro-ph/9910075)

Jørgensen, I., & Franx, M. 1994, ApJ, 433, 553

Jørgensen, I., Franx, M., Hjorth, J., & van Dokkum, P. G. 1999, MNRAS, 308, 833

Kelson, D. D., van Dokkum, P. G., Franx, M., Illingworth, G. D., & Fabricant, D. 1997, ApJ, 478, L13

Kelson, D. D., Illingworth, G. D., van Dokkum, P. G., & Franx, M. 2000, ApJ, in press (astro-ph/9906152)

Kodama, T., Arimoto, N., Barger, A. J., & Aragon-Salamanca, A. 1998, A&A, 334, 99

Krist, J. 1995, in Astronomical Data Analysis Software and Systems IV, ASP Conference Series, 77, R. A. Shaw, H. E. Payne, and J. J. E. Hayes, eds., p. 349

Lavery, R. J., Pierce, M. J. & McClure, R. D. 1992, AJ, 104, 2067

Lilly, S. 1993, ApJ, 411, 501

Liu, C. T., & Kennicutt, R. C., Jr. 1995, ApJ, 450, 547

Lubin, L. M., Postman, M., Oke, J. B., Ratnatunga, K. U., Gunn, J. E., Hoessel, J. G., & Schneider, D. P. 1998, AJ, 116, 584

Luppino, G. A., & Kaiser, N. 1997, ApJ, 475, 20

Moore, B., Lake, G. & Katz, N. 1998, ApJ, 495, 139

Oemler, A., Jr. 1974, ApJ, 194, 1

Oemler, A., Jr., Dressler, A. & Butcher, H. R. 1997, ApJ, 474, 561

Oke, J. B., Cohen, J. G., Carr, M., Cromer, J., Dingizian, A., Harris, F. H., Labrecque, S., Lucinio, R., Schaaf, W., Epps, H., & Miller, J. 1995, PASP, 107, 375

Osterbrock, D. E., Fulbright, J. P., Martel, A. R., Keane, M. J., Trager, S. C., & Basri, G. 1996, PASP, 108, 277

Pahre, M. 1998, Ph.D. thesis, California Institute of Technology

Poggianti, B., Smail, I., Dressler, A., Couch, W., Barger, A., Butcher, H., Ellis, R., & Oemler, A., Jr. 1999, ApJ, 518, 576

Postman, M., Lubin, L. M., & Oke, J. B. 1998, AJ, 116, 560

Postman, M. 1999, in Clustering at High Redshift, Marseilles, in press (astro-ph/9910473)

Rakos, K. D., & Schombert, J. M. 1995, ApJ, 439, 47

Rix, H.-W., & White, S. D. M. 1990, ApJ, 362, 52

Salpeter, E. 1955, ApJ, 121, 161

Smail, I., Hogg, D. W., Yan, L., & Cohen, J. G. 1995, ApJ, 449, L105

Smail, I., Dressler, A., Couch, W. J., Ellis, R. S., Oemler, A., Jr., Butcher, H., & Sharples, R. M. 1997, ApJS, 110, 213

Smail, I., Edge, A. C., Ellis, R. S., & Blandford, R. D. 1998, MNRAS, 293, 124

Solanes, J. M. & Salvador-Sole, E. 1992, ApJ, 395, 91

Stanford, S. A., Eisenhardt, P. R. M., & Dickinson, M. 1995, ApJ, 450, 512

Stanford, S. A., Eisenhardt, P. R., & Dickinson, M. 1998, ApJ, 492, 461

Tran, K.-V. H., Kelson, D. D., van Dokkum, P. G., Franx, M., Illingworth, G. D., & Magee, D. 1999, ApJ, 522, 39

Tytlar, D. & Vidal, N. V. 1978, MNRAS, 182, 33P

Valdes, F. G., Campusano, L. E., Velasquez, J. D., & Stetson, P. B. 1995, PASP, 107, 1119

van Dokkum, P. G., & Franx, M. 1996, MNRAS, 281, 985

van Dokkum, P. G., Franx, M., Kelson, D. D., Illingworth, G. D., Fisher, D., & Fabricant, D. 1998a, ApJ, 500, 714

van Dokkum, P. G., Franx, M., Kelson, D. D., Illingworth, G. D. 1998b, ApJ, 504, L17

van Dokkum, P. G., Franx, M., Fabricant, D., Kelson, D. D., Illingworth, G. D. 1999, ApJ, 520, L95

Worley, G. 1994, ApJS, 95, 107

Yee, H. K. C., Ellingson, E., Abraham, R. G., Gravel, P., Carlberg, R. G., Smecker-Hane, T. A., Schade, D., & Rigler, M. 1996, ApJS, 102, 289

TABLE 3  
OFFSET AND SCATTER OF THE CM RELATION

Sample	<i>N</i>	Offset	Error	Obs. Scatter	Error
E+S0	30	0.000	0.005	0.029	0.005
S	26	-0.219	0.047	0.255	0.025
M/P	13	-0.066	0.019	0.074	0.040
E+S0+M/P	43	-0.008	0.007	0.050	0.013
All	81	-0.018	0.008	0.081	0.029

TABLE 1  
SPECTROSCOPIC DATA

Id	<i>z</i>	H $\delta$	$\pm$	O II	$\pm$	type	Id	<i>z</i>	H $\delta$	$\pm$	O II	$\pm$	type
514	0.8398	-2.5	3.0	4.4	3.2	abs	1439	0.8213	4.2	2.8	2.3	2.6	E+A?
564	0.8322	3.2	4.0	-39.0	6.8	emi	1457	0.8420	2.7	1.2	3.8	1.3	abs
573	0.8362	3.7	2.8	-1.0	3.1	abs?	1459	0.8461	5.6	0.9	-5.9	1.2	emi?
661	0.8470	1.0	2.1	-5.4	2.2	emi?	1477	0.8274	1.2	2.6	-4.5	3.0	abs?
675	0.8417	3.2	2.3	-1.9	3.1	abs?	1481	0.8258	-0.6	2.0	4.4	2.0	abs
696	0.8317	1.3	1.2	1.4	1.5	abs	1484	0.8318	1.0	1.0	0.1	1.2	abs
696	0.8322	1.4	1.4	0.2	1.5	abs	1486	0.8332	0.1	3.4	3.8	4.0	abs
703	0.8323	-0.5	3.8	1.1	3.7	abs	1492	0.8280	1.1	2.4	1.1	2.5	abs
710	0.8344	0.4	1.2	-1.2	1.5	abs	1493	0.8334	2.9	2.9	-0.6	3.6	abs?
742	0.8307	0.3	2.7	-2.7	3.0	abs?	1519	0.8301	1.4	2.1	4.5	2.3	abs
777	0.8323	3.7	1.6	2.9	1.9	abs?	1520	0.8310	0.1	2.7	-1.5	2.8	abs
793	0.8276	5.3	2.6	-2.4	3.1	E+A?	1567	0.8279	3.4	1.3	2.3	1.4	abs?
796	0.8235	2.9	1.6	0.8	1.8	abs?	1583	0.8261	6.9	0.6	-0.4	0.7	E+A
997	0.8389	0.2	0.7	-1.0	0.8	abs	1584	0.8313	-0.4	1.6	-1.1	2.1	abs
1035	0.8307	8.1	2.4	-4.3	2.9	E+A?	1585	0.8369	4.4	3.1	-3.8	3.3	E+A?
1088	0.8184	1.0	2.5	3.1	2.1	abs	1635	0.8363	1.3	1.7	1.7	2.7	abs
1091	0.8449	3.7	1.6	-4.6	2.5	abs?	1639	0.8377	5.4	2.0	-8.1	2.3	emi
1103	0.8222	5.7	1.9	-5.0	1.9	E+A?	1650	0.8297	8.8	2.1	-6.3	2.4	emi?
1114	0.8317	0.5	2.2	2.1	2.6	abs	1650	0.8294	7.1	2.8	-3.9	3.1	E+A?
1119	0.8225	-4.2	3.0	4.1	2.3	abs	1651	0.8241	0.7	3.5	3.4	3.6	abs?
1163	0.8338	3.7	1.2	-1.1	1.7	abs?	1656	0.8223	2.0	1.3	-0.2	1.5	abs
1198	0.8313	1.7	2.4	-5.2	2.9	emi?	1692	0.8253	1.7	2.9	-1.6	3.0	abs?
1209	0.8376	2.5	1.5	-0.4	2.0	abs?	1701	0.8317	1.2	1.7	3.7	2.0	abs
1215	0.8394	2.2	1.7	-3.4	2.3	abs?	1733	0.8347	0.5	4.9	-23.0	5.6	emi
1280	0.8372	0.4	1.3	0.3	1.7	abs	1758	0.8374	5.1	2.4	3.0	3.4	E+A?
1294	0.8352	-2.5	1.0	0.3	1.1	abs	1760	0.8246	5.6	1.2	-1.3	1.4	E+A
1298	0.8363	1.5	2.7	-5.9	4.3	emi?	1763	0.8390	3.9	4.1	-20.8	4.7	emi
1304	0.8335	2.6	1.3	0.4	1.6	abs	1801	0.8328	0.6	1.1	-51.9	1.6	emi
1325	0.8311	2.1	1.0	0.8	1.2	abs	1834	0.8394	7.6	1.3	-3.1	1.8	E+A
1329	0.8352	3.2	2.5	-3.5	3.8	abs?	1855	0.8210	2.7	2.4	-17.8	3.8	emi
1355	0.8355	1.1	1.3	2.5	1.7	abs	1896	0.8227	2.5	3.4	-20.6	3.1	emi
1359	0.8180	0.9	1.7	1.7	1.6	abs	1929	0.8400	2.8	1.5	2.7	1.7	abs?
1396	0.8299	-2.6	2.1	3.5	2.6	abs	1942	0.8307	1.8	1.2	-2.1	1.5	abs
1403	0.8132	2.8	1.9	-14.7	2.2	emi	1986	0.8253	0.4	1.5	-0.1	1.7	abs
1405	0.8363	1.2	1.4	-0.6	2.0	abs	2011	0.8413	-4.2	3.2	-32.5	3.4	emi
1406	0.8206	-2.2	1.8	-2.8	1.8	abs	2130	0.8250	3.1	4.2	-10.2	4.5	emi
1422	0.8330	-2.8	2.9	-2.5	2.2	abs	2152	0.8319	-0.8	1.0	-2.8	0.8	abs
1430	0.8240	5.4	1.2	0.3	1.3	E+A	2174	0.8382	-1.6	2.6	2.4	3.3	abs
1434	0.8248	-1.8	2.3	4.5	2.0	abs	HES1 <sup>a</sup>	0.8286	-11.8	9.2	-66.5	14.9	emi
1435	0.8197	0.9	2.6	0.8	2.7	abs	HES2 <sup>a</sup>	0.8240	-1.4	5.8	-64.0	11.9	emi

NOTE.—<sup>a</sup> Galaxies unintentionally covered by slits pointed at other objects. These objects have  $I \sim 24$  and were not in the photometric catalog.

TABLE 2  
PHOTOMETRIC DATA

Id	morph	$F814W^T$	$B_z^T$	$(U-B)_z$	$\Delta(U-B)_z$	Id	morph	$F814W^T$	$B_z^T$	$(U-B)_z$	$\Delta(U-B)_z$
514	M/P	21.83	23.00	0.402	-0.022	1434	E/S0	21.96	23.13	0.410	-0.010
661	Sc	21.05	22.24	-0.064	-0.512	1435	E/S0	21.87	23.04	0.366	-0.057
675	M/P	21.36	22.53	0.393	-0.046	1439	?	21.97	23.14	0.461	0.042
696	S0/a	20.55	21.72	0.467	0.002	1457	M/P	21.00	22.17	0.448	-0.003
703	?	21.91	23.08	0.360	-0.061	1459	Sc	20.66	21.84	0.183	-0.278
710	E	20.78	21.95	0.432	-0.026	1477	S0/a	21.57	22.74	0.378	-0.055
777	S0	20.99	22.16	0.431	-0.020	1478	Sa	21.37	22.54	0.496	0.057
793	M/P	21.14	22.31	0.365	-0.082	1481	S0	21.95	23.12	0.373	-0.047
796	S0	21.80	22.97	0.413	-0.012	1484	E	19.53	20.70	0.496	-0.002
997	M/P	20.29	21.47	0.343	-0.130	1486	Sa	22.00	23.17	0.534	0.116
1024	?	21.75	22.95	-0.194	-0.619	1492	?	21.95	23.12	0.440	0.020
1035	M/P	22.34	23.53	-0.122	-0.528	1493	Sb	22.30	23.47	0.454	0.045
1039	Sa	21.31	22.49	0.333	-0.108	1519	S0/a	21.21	22.38	0.454	0.010
1043	E	20.87	22.04	0.461	0.006	1520	E/S0	21.57	22.74	0.442	0.009
1086	S0	21.65	22.82	0.424	-0.006	1567	E	21.04	22.21	0.494	0.044
1088	E	21.92	23.09	0.423	0.002	1583	M/P	20.50	21.68	0.318	-0.149
1091	S0	22.05	23.23	0.215	-0.201	1584	E	20.76	21.93	0.483	0.024
1103	E/S0	21.95	23.14	0.059	-0.361	1585	Sc	22.09	23.28	0.004	-0.411
1114	S0/a	21.44	22.61	0.410	-0.027	1635	S0/a	21.77	22.94	0.467	0.041
1119	S0	21.85	23.02	0.442	0.019	1639	Sb	21.59	22.77	0.200	-0.232
1163	M/P	20.49	21.66	0.438	-0.029	1650	Sd	21.59	22.78	0.056	-0.375
1198	Sa	22.17	23.36	0.031	-0.381	1651	E/S0	22.17	23.34	0.463	0.050
1209	S0	21.41	22.58	0.504	0.066	1655	E	20.94	22.12	0.252	-0.200
1215	Sa	21.09	22.26	0.421	-0.027	1656	E/S0	21.06	22.23	0.448	-0.001
1280	E	20.74	21.91	0.482	0.022	1692	M/P	21.68	22.86	0.313	-0.115
1294	E/S0	20.60	21.77	0.472	0.008	1701	S0	21.10	22.27	0.447	-0.001
1298	Sa	22.11	23.28	0.469	0.054	1733	Sc	22.07	23.26	-0.036	-0.452
1304	Sb	21.28	22.45	0.396	-0.046	1758	S0/a	21.93	23.11	0.354	-0.066
1305	Sb	22.04	23.22	0.335	-0.082	1760	M/P	20.29	21.46	0.369	-0.105
1325	E	19.88	21.05	0.478	-0.009	1763	Sb	22.71	23.90	-0.086	-0.481
1329	Sb	20.87	22.04	0.393	-0.062	1801	M/P	20.39	21.60	-0.536	-1.005
1340	M/P	21.06	22.23	0.472	0.023	1834	Sb	20.98	22.16	0.326	-0.125
1354	Sb	21.51	22.68	0.424	-0.010	1896	Sc	21.12	22.32	-0.210	-0.656
1355	E/S0	21.38	22.55	0.455	0.017	1929	E	21.18	22.35	0.410	-0.035
1359	E/S0	21.09	22.26	0.457	0.010	1942	E/S0	20.98	22.15	0.457	0.006
1396	S0/a	21.60	22.77	0.486	0.055	1986	Sb	21.30	22.47	0.524	0.083
1403	Sc	20.14	21.33	-0.037	-0.515	2011	M/P	22.13	23.33	-0.271	-0.685
1405	E	20.03	21.20	0.478	-0.004	2130	Sd	21.84	23.03	-0.001	-0.424
1406	E	21.42	22.59	0.398	-0.040	2174	S0/a	21.82	22.99	0.372	-0.052
1422	Sc	21.03	22.23	-0.230	-0.679	HES1	Sd	23.21	24.23	-0.194	-0.752
1430	Sb	20.36	21.54	0.348	-0.123						